Vibrational Dynamics of a Metalloporphyrin Carbonyl in Liquid and Glass Solutions: Ultrafast 1-D and Frequency-Selected Vibrational Echo Experiments

Qing-Hua Xu and M. D. Fayer

Department of Chemistry, Stanford University, Stanford, CA, 94305 USA
e-mail: fayer@zog.stanford.edu
Received January 17, 2002

Abstract—One-dimensional and frequency-selected ultrafast infrared vibrational echo experiments on the CO stretching mode of a metalloporphyrin carbonyl compound in poly-methylmethacrylate (PMMA) and in 2-methylteterahydrofuran (2-MTHF) were compared. By selecting the proper detection wavelengths, the frequency-selected vibrational echo permits the independent detection of the dephasing dynamics associated with 0–1 and 1–2 vibrational transitions, eliminating cross terms and anharmonic beats that occur in the 1D echo signals. In PMMA, the dephasing dynamics associated with the 0–1 transition are single exponential at low and high temperatures, suggesting motional narrowed homogeneous dephasing imbedded in a massively inhomogeneously broadened line. In 2-MTHF liquid, 0–1 transition dephasing dynamics are exponential at low temperature, but, the are non-exponential at high temperatures, demonstrating that a variety of time scales of solvent fluctuations contribute to the dephasing dynamics. In the high temperature 2-MTHF liquid, 0–1 and 1–2 dephasing dynamics are essentially identical. Aspects of the negative delay time signals are also discussed.

1. INTRODUCTION

In this paper, one-dimensional (1-D) ultrafast infrared vibrational echoes and frequency-selected vibrational echoes (a type of frequency-dispersed experiment) are employed to study solute-solvent dynamic interactions of a molecule in both liquid and solid solutions. The vibrational echo is the infrared vibrational equivalent of the NMR spin echo [1] and the electronic transition photon echo [2–4]. With the advent of the ultrafast infrared vibrational echo [5], the gap between the radio frequency spin echo and the visible and ultraviolet electronic excited state photon echo was filled. The spin echo, the vibrational echo, and the photon echo comprise three of the most important members of the family of non-linear techniques that exploit the interaction of the molecules and electromagnetic fields.

Nonlinear spectroscopic techniques have proven useful in the study of molecular systems because they enable information to be obtained that cannot be extracted readily from a linear spectrum. Studies of solute-solvent interaction dynamics have shown that many dynamical processes can occur on the picosecond and femtosecond time scales [6]. For the study of such fast time scale processes, NMR spin echo studies are limited by the intrinsic NMR time scale, typically microsecond. The electronic transition photon echo and other visible optical nonlinear experiments have benefited from the recent rapid developments and applications of ultrashort pulses [7]. However, resonant nonlinear experiments involving electronic transitions are complicated by molecular vibrations that give rise to vibrational progressions in the electronic absorption spectrum. Intramolecular vibrational modes have a signifi-

cant influence on third-order nonlinear signals [8, 9]. The complexity brought on by the simultaneous excitation of many vibronic transitions can make it difficult to analyze the results of ultrafast nonlinear experiments involving electronic transitions [9, 10].

The ultrafast infrared vibrational echo experiment [11–22], can overcome the limitations of its two analogs. Recent developments of ultrafast IR pulses have enabled the vibrational echo to probe dynamics on femtosecond time scales. Vibrational echo experiments are providing significant information on liquids [12, 14, 20–22], glasses [12, 14], and proteins [23–28]. Recent advances using two-dimensional methods [15–18, 20–22], are increasing the utility of the vibrational echo technique.

It is possible to perform a vibrational echo experiment on a single vibrational fundamental if a relatively long (narrow bandwidth) pulse is used [29]. However, to achieve the high temporal resolution, the broad spectral bandwidth that is required to generate ultrashort pulses, will usually span both 0–1 (fundamental) and 1–2 transitions unless the anharmonicity of the vibration is very large. The 1–2 transition will be involved in a third-order signal. The additional contribution of the 1–2 transition to the vibrational echo signal makes the observed signal more complex and more difficult to interpret than a signal arising from a system involving only two states (the ground state and the first excited vibrational state) [17, 19, 30, 31]. In a one dimensional echo experiment, the interference of the different excitation pathways that occur in a multilevel system will produce non-exponential decays that can also display anharmonic beats [17, 19, 30, 31] even if the dynamic dephasing of the individual transitions is exponential. If

the individual decays are intrinsically non-exponential, then the 1-D signal is virtually impossible to separate into its components.

2-D vibrational echo experiments, in which the vibrational echo pulse is frequency-resolved, have been used to reveal the nature of the quantum beats, anharmonic beats, and accidental degeneracy beats [19]. In a spectrally resolved 2-D vibrational echo experiment, a two-dimensional, time-frequency, spectrum is recorded [15, 17, 18, 32]. While full 2-D vibrational echo spectroscopy can provide a variety of types of information that cannot be obtained from a 1-D experiment, in many applications, what is desired is the equivalent of a 1-D experiment, but a 1-D experiment that is free from the complications that arise from the interference effect in a multilevel system. Below, it will be demonstrated that by selecting the proper detection wavelengths of the vibrational echo signal, which is equivalent to taking the appropriate slices through the 2-D spectrum, it is possible to obtain the ultrafast dynamics associated with either the 0–1 or 1–2 transitions separately, eliminating cross terms and anharmonic beats [30, 31]. Thus, the signal can be modeled as arising from a simple two-level system even though the broad bandwidth associated with the ultrafast excitation pulses spans more than two levels. This technique permits the study of the underlying dynamics without the complications brought on by the anharmonicity or other multi-level affects.

The utility of this technique is demonstrated for the CO stretching mode of a metalloporphyrin carbonyl compound (a model scheme), RuTPPCOPy (TPP = 5,10,15,20-tetraphenylporphyrin, Py = pyridine), in two solvents, poly-methylmethacrylate (PMMA) and 2-methyltetarahydrofuran (2-MTHF). PMMA is a glass at all temperatures studied, while 2-MTHF is a glass forming liquid with its glass transition temperature at 86 K. In contrast to other metal-carbonyl systems that have been studied [13, 14, 17, 29], this system has a single CO mode that is non-degenerate. Therefore, complications produced by quantum beats and those associated with line broadening mechanisms that can arise from degeneracies are avoided. In PMMA, the inhomogeneous line is broad, and there is substantial overlap between the 0–1 and 1–2 transitions, producing strong anharmonic beats in the 1-D vibrational echo decay. These are eliminated through the proper choice of detection wavelength. In 2-MTHF, the absorption line is narrower, and there is little overlap between the 0–1 and 1–2 transitions. No beats are observed in the 1-D spectrum, consistent with theoretical prediction [17, 19]. The vibrational echo decays in the high temperature liquid are non-exponential and virtually identical for 0–1 and 1–2 transitions. There is a strong signal at negative time delays, which is stronger for a detection wavelength on the 1–2 transition than for detection on the 0–1 transition. In the 2-MTHF solvent, a strong signal at negative delay times is also observed because the inhomogeneous line width is narrow.
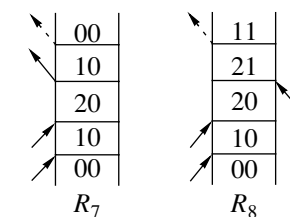
(a) Positive delay time diagrams, k_1–k_2–k_2
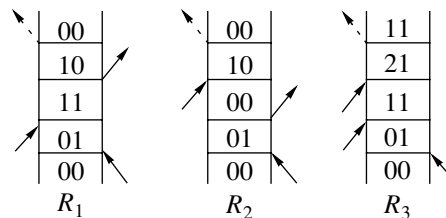
(b) Pulse overlap diagrams, k_2–k_1–k_2
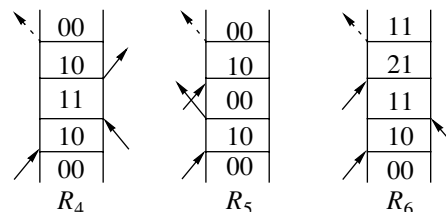
(c) Negative delay time diagrams, k_2–k_2–k_1

Fig. 1. Double-sided Feynman diagrams for a vibrational echo for a three-level system. Because it is a third order phenomenon, only three levels contribute to a vibrational echo signal detected in the phase matched direction. (a) R_1, R_2 and R_3 are for positive delay times; (b) R_4, R_5 and R_6 for times when the pulses overlap; (c) R_7 and R_8 for negative delay times.

2. 1-D AND FREQUENCY-SELECTED VIBRATIONAL ECHO (FSVE)

For femtosecond third-order IR experiments, the bandwidth of the femtosecond IR pulse is usually broad enough to cover both 0–1 and 1–2 transitions. Thus the $v = 2$ vibrational level will also be involved in the experiments. A three-level system is necessary to model the vibrational echo experiments performed on vibrational transitions of molecules.

For a three-level system, eight double-sided Feynman diagrams (Fig. 1), which exist after making the rotating wave approximations, will contribute to the total signal in a two-pulse vibrational echo experiment [33, 34]. In the experiments, the two pulses are separated by a variable time delay τ. Three diagrams are for the positive time delay region, that is, $\tau > 0$ (R_1, R_2 and R_3), three are for the pulse overlap region, $\tau \cong 0$ (R_4, R_5, and R_6), and two are for the negative time delay region, $\tau < 0$ (R_7 and R_8). For τ much greater than the pulse duration, only R_1, R_2 and R_3 will contribute to the echo signal. Of these three, R_1 and R_2 involve the 0–1 transition only; however, R_3 also involves the 1–2 transition

[33]. Among these diagrams, only four of them (R_1, R_2, R_4, and R_5) will contribute if the system is rigorously a two-level system (only the 0–1 transition is involved). This situation will arise if the anharmonicity is much greater than the pulse bandwidth and there are no other vibrational transitions coupled to the ground state that can give rise to quantum beats and anharmonic beats [19]. When the delay is much longer than the pulse duration, only the positive terms (R_1, R_2, and R_3 for a three-level system, and R_1 and R_2 for a two-level system) need to be considered.

The homodyne echo signal measured by a slow detector can be written as the integrated modulus squared of third-order polarization [33].

$$S(\tau) \propto \int_0^\infty \left| P^{(3)}(\tau, t) \right|^2 dt, \qquad (1)$$

where the third-order polarization $P^{(3)}$ is the convolution of the electric fields with the response functions, R. In the impulsive limit, $P^{(3)} \propto R$ and the total response function $R = \sum R_i$. R_i contains the dynamical information involved in the calculation of the different double-sided Feynman diagrams shown in Fig. 1.

The response function can be calculated through line broadening function $g(t)$, which connects the non-linear response and the linear spectrum. The linear absorption spectrum is usually calculated by [33]

$$I(\omega) = \text{Re} \int_0^\infty dt \exp[-(\omega - \omega_{01})t - g(t)]. \qquad (2)$$

The calculation of the nonlinear response has been discussed in detail in the monograph by Mukamel [33]. For vibrational transitions, $g(t)$ is usually assume to be real since no time dependent spectral shift was yet seen in the pump probe experiments. The total response function for positive delay times can be represented by

$$R = \sum_{i=1}^{3} R_i = 2R_1(\tau, t)(1 - e^{i\Delta t}), \qquad (3)$$

where $R_1(\tau, t) = \exp(-2g(\tau) - 2g(t) + g(\tau + t))$ and Δ is the anharmonic shift, that is, the difference in frequency between the 0–1 and 1–2 transitions. $g(t)$ can be calculated from frequency-frequency correlation function, which describes the solvent and solute interactions,

$$g(t) = \int_0^t d\tau_1 \int_0^{\tau_1} d\tau_2 \langle \delta\omega_{10}(\tau_2)\delta\omega_{10}(0) \rangle. \qquad (4)$$

In Eq. (3), it is assumed that the fluctuations of the 0–1 and 1–2 transitions are fully correlated, i.e., $\delta\omega_{12} = \delta\omega_{01}$. Thus, the total echo signal in the impulsive limit can be described by

$$S(\tau) \propto \int_0^\infty \left| R_1(\tau, t)(1 - e^{i\Delta t}) \right|^2 dt. \qquad (5)$$

The 2-D or frequency-dispersed echo signal can be calculated by the square of the Fourier transformed $P^{(3)}$ along t axis.

$$S(\tau, \omega) \propto \left| \int e^{i\omega t} P^{(3)}(\tau, t) dt \right|^2 \qquad (6a)$$

$$\propto \left| \int e^{i\omega t} R_1(\tau, t)(1 - e^{i\Delta t}) dt \right|^2$$

$$= \left| \int e^{i\omega t} R_1(\tau, t) dt - \int e^{i(\omega + \Delta)t} R_1(\tau, t) dt \right|^2. \qquad (6b)$$

In Eq. (6b), the first term peaks at ω_{10}, corresponding to the echo spectrum of the 0–1 transition (R_1 and R_2); the second term peak at $\omega_{21} = \omega_{10} - \Delta$, corresponding to the echo spectrum of the overtone absorption (R_3). From Eq. (6), it can be seen that by choosing the proper detection frequency ω, it is possible to suppress one of the terms and avoid the interference. Therefore, the contributions from either R_1/R_2 (which are identical) or R_3 can be obtained separately.

The above discussion only considers the pure dephasing process (contributions from the solute—solvent interactions) and the lifetime effect is not included. In the vibrational transition case, vibrational relaxation may contribute significantly to the total dephasing (see experiments discussed below); the lifetime needs to be included. In Eq. (2), different response function terms need to be scaled by the corresponding population contribution: $\exp[-(t + \tau)/2T_{l, v=1}]$ for the R_1 and R_2 terms,

and $\exp\left[-(\tau/2T_{l, v=1}) - t/\left(\dfrac{1}{2T_{l, v=1}} + \dfrac{1}{2T_{l, v=2}} \right) \right]$ for

the R_3 term.

3. EXPERIMENTAL PROCEDURES

The experimental apparatus for the ultrafast infrared vibrational echo has been described in detail previously [17]. Briefly, tunable mid-IR pulses centered at 1948 cm^{-1} with a repetition rate of 1 kHz were generated by an optical parametric amplifier pumped with a regeneratively amplified Ti:Sapphire laser. The bandwidth and pulse duration of the pulses were 90 cm^{-1} (FWHM) and 170 fs (FWHM). Both the time profile and the pulse spectrum were essentially Gaussian in shape, and the pulses were nearly transform limited (time-bandwidth product = 0.46). A 15/85% ZnSe beam splitter was used create a weak beam (wave vector $\mathbf{k}_1$) and strong beam (wave vector $\mathbf{k}_2$). In a two-pulse vibrational echo experiment, the signal intensity is linear in the intensity of the first pulse and quadratic in the intensity of the second pulse. Therefore, it is advantageous to have the second pulse more intense than the first pulse. Furthermore, to perform a pump-probe measurement of the vibrational lifetime, the probe pulse should be weak compared to the pump pulse. The 15/85% ZnSe beam splitter makes it possible to do both experiments without changing optics. The weak beam

was delayed with respect to the strong beam by a stepper-motor translation stage. The beams were crossed and focused at the sample to a spot size of 150 μm. The vibrational echo signal was generated in the phase matched direction $-\mathbf{k}_1 + 2\mathbf{k}_2$, and was detected with a liquid nitrogen cooled HgCdTe detector directly (for 1-D signal) or first passed through a monochromator (frequency selected signal). The resolution of the monochromator was set to 2 cm^{-1}. The pulse energy was ~3.5 μJ/pulse (before the beam splitter). Detailed power studies were performed to make sure that there were no higher order effects and no heating effects.

RuTPPCO, PMMA, methylene chloride (CH$_2$Cl$_2$) were purchased from Aldrich and used without further purification. The 2-MTHF (Aldrich) was dried and distilled before use. The RuTPPCOPy/2-MTHF solution was prepared by dissolving the RuTPPCO in 2-MTHF and then adding two-fold excess of pyridine into the RuTPPCO solution. Pyridine is the 5th ligand on the Ru. The optical density (OD) of the CO stretching mode in the 200 μm path length sample cell was of 0.1. The PMMA glass film was prepared by mixing PMMA with a RuTPPCOPy/CH$_2$Cl$_2$ solution. The solution was spread on a clean glass plate and dried under a closed atmosphere for two days. The sample was then placed under vacuum for a week to remove the remaining solvent. The thickness of the PMMA film sample was 150 to 200 μm, and the OD was ~0.5 at the absorption maximum. The samples were placed between two CaF$_2$ windows in a custom gas-tight copper sample cell. The temperature of the sample was controlled with a continuous flow cryostat and monitored with a silicon diode temperature sensor bonded to the front CaF$_2$ window.

4. RESULTS AND DISCUSSION

4.1. FSVE Study of RuTPPCOPy in PMMA Polymer Matrix

Figure 2 shows the 1-D vibrational echo data for RuTPPCOPy in PMMA at three different temperatures: 80, 180, and 280 K (from top to the bottom). The decays of 1-D signals are multi-exponential and are modulated by oscillatory beats at all three temperatures. The echo decay becomes slower and the oscillatory modulation becomes stronger as the temperature decreases. The oscillatory beats are described in terms of the interference of the R_1/R_2 terms with the R_3 term, which produces a beat at the frequency difference between 0–1 and 1–2 transitions, that is, the anharmonic shift [17, 19, 30, 31]. Such beats are referred to as anharmonic beats [17, 19, 30, 31]. An important prerequisite for the observation of the anharmonic beats is the substantial spectral overlap between the spectra of the 0–1 and 1–2 transitions. In the current system, the inhomogeneity (~22 cm^{-1}) is comparable to the vibrational anharmonicity (25 cm^{-1}), which was determined from the beat frequency [30, 31].

Signal, arb. units
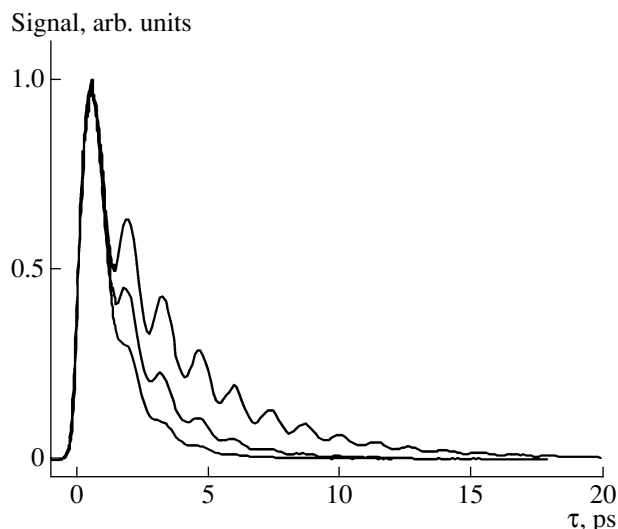
Fig. 2. 1-D vibrational echo decays of RuTPPCOPy in PMMA at 80, 180, and 280 K (from top to the bottom). The bandwidth of the pulse is much larger than the anharmonic shift of the 1–2 transition (25 cm^{-1}) to lower energy than the 0–1 transition. The decay is a tri-exponential with anharmonic beats, that is, beats at the difference in the 0–1 and 1–2 transition frequencies.

Figure 3 displays the 0–1 spectrum (fundamental) and 1–2 spectrum at 80 K. The 1–2 spectrum was modeled as the 0–1 spectrum shifted by the anharmonicity. The spectrally resolved pump-probe experiments on metal carbonyls by Heilweil *et al.* [35] have shown that the absorption spectra of the fundamental and the 1–2 transition have similar linewidths. It is reasonable to assume that the linewidths are identical for the two transitions for the current system. Figure 3 displays substantial spectral overlap between 0–1 and 1–2 transition in PMMA at 80 K. The linewidth of the 0–1 absorption spectrum was also found to be insensitive to the temperature in the range between 60 and 300 K. The anharmonic shift obtained from the beats in the 1-D echo signal (Fig. 2) was found to be identical for three different temperatures, demonstrating that the anharmonicity is not dependent on temperature.

In a 1-D vibrational echo experiment, even if the decays associated with R_1/R_2 and R_3 terms are individually distinct single exponentials (as in PMMA solvent, see below), the interference of these terms will cause the total signal to be a tri-exponential with beats. The time constants associated with the individual terms are difficult to resolve, especially when the time constants are similar. If the individual decays are non-exponential and the functional form is not known (as in the case of RuTPPCOPy in 2-MTHF solvent at high temperatures), then it is virtually impossible to separate the distinct decay components.

The problems associated with the 1-D data (Fig. 2) can be overcome by performing a frequency selected vibrational echo (FSVE). By selecting the proper detection wavelengths, it is possible to obtain the con-
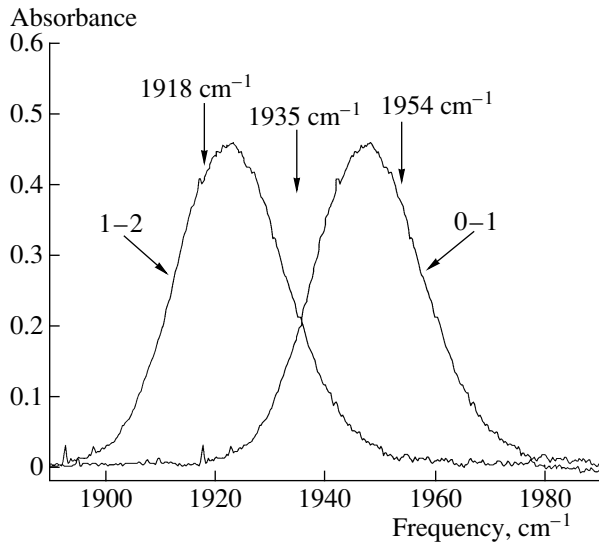
Fig. 3. The absorption spectrum of RuTPPCOPy in PMMA at 80 K labeled 0–1. The curve labeled 1–2 is a model of the 1–2 absorption spectrum obtained by shifting the 0–1 spectrum by the anharmonic shift of 1–2 transition (25 cm^{-1}), which was determined from the beat frequency in Fig. 2. The frequencies indicated with errors correspond to the observations frequencies for the data presented in Fig. 4.

tribution to the signal corresponding solely to R_1/R_2 or R_3 terms, removing the contamination from other terms. Frequency selected echo experiments are shown for three different detection wavelengths, 1954, 1935, and 1918 cm^{-1} in Fig. 4. The data displayed in Fig. 4 were taken at the three wavelengths indicated in Fig. 3. The data in Fig. 4a were taken slightly on blue side of center 0–1 transition (1954 cm^{-1}), the data in Fig. 4b were taken half way between the two transitions (1935 cm^{-1}), and the data in Fig. 4c were taken slightly on red side of the 1–2 transitions (1918 cm^{-1}). In Fig. 4b, the beats are very pronounced with almost 100% modulation depth. In this case, both R_1/R_2 and R_3 terms contribute almost equally to the signal, producing strong anharmonic beats at positive delay times. When the blue wavelength is selected (Fig. 4a), the echo signal is dominated by the contribution from the R_1/R_2 terms, and the contribution from R_3 term is suppressed; the interference is essentially eliminated. The decay shown in Fig. 4a (1954 cm^{-1}) is for the pure 0–1 transition. At positive delay times, it is equivalent to the pure two level (0–1 transition) vibrational echo decay. Similarly, when the red wavelength (1935 cm^{-1}, Fig. 4c) is selected, the signal is dominated by the contribution from R_3 term, free of the contamination from R_1/R_2 terms. At both wavelengths, the oscillations are virtually eliminated, and the echo decays can be fit with single exponentials, as shown in the insets.

The decay rate associated with R_3 (Fig. 4c) is faster than that of R_1/R_2 (Fig. 4a). In a Bloch picture, the decay rates of the signal associated with R_1 and R_2
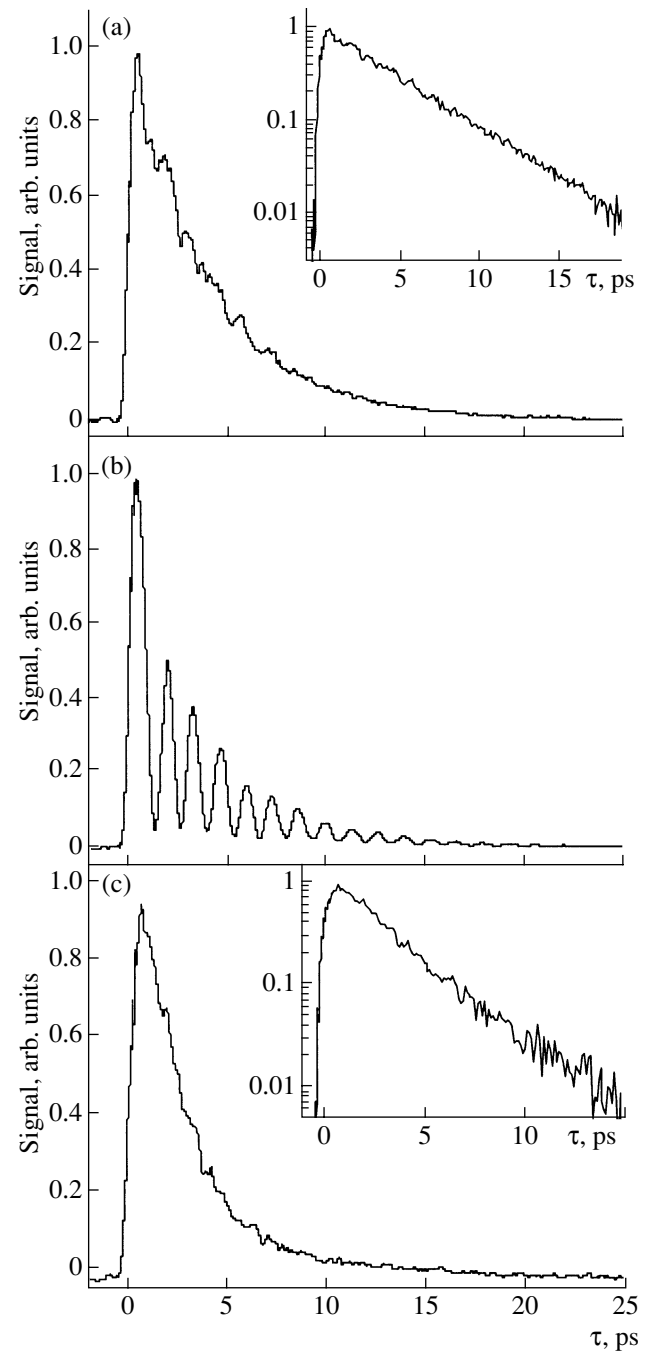
Fig. 4. Frequency-selected vibrational echo decays (slices through the 2-D spectrum) of the CO stretch of RuTPPCOPy in PMMA at 80 K. (a) 1954 cm^{-1}, the 0–1 transition; (b) 1935 cm^{-1}, between the 0–1 and 1–2 transitions; (c) 1918 cm^{-1}, the 1–2 transition. The wavelengths are indicated with arrows in Fig. 3. Almost 100% modulation is seen at 1935 cm^{-1}, where the 0–1 and 1–2 spectra overlap (see Fig. 3). At the other two frequencies, single exponential decays (see insets) are observed.

terms are identical and are denoted by $4\gamma_{01}$, while the decay rate associated with the R_3 term is $(2\gamma_{01} + 2\gamma_{12})$, where γ_{01} and γ_{12} denote the total dephasing rates asso-

ciated with the 0–1 and 1–2 transition, respectively. The data demonstrate that the total dephasing rate associated with 1–2 transition is faster than that of R_1/R_2 terms, that is, $\gamma_{01} = 1/(16.0 \text{ ps})$ and $\gamma_{12} = 1/(7.0 \text{ ps})$ at 80 K. The total dephasing process has contributions from both vibrational population relaxation and pure dephasing processes. The higher vibrational levels in general have shorter lifetimes than that of $v = 1$ level. For a harmonic oscillator, the lifetime of a vibration level is inversely proportional to its quantum number, while the pure dephasing is only dependent on the difference between the quantum numbers of the levels involved [36]. For a system with a small anharmonicity, it is reasonable to assume that the pure dephasing rates associated with 0–1 and 1–2 transitions are very similar, which was found to be in other systems [15] and in the systems studied here at high temperatures. The vibrational lifetime is sensitive to the anharmonic coupling, and the ratio of relaxation rate of higher vibrational levels to that of the $v = 1$ level is generally greater than that predicted for a harmonic oscillator [37]. At low temperatures, the vibrational population decays of the levels make a significant contribution to the total dephasing [14, 31]. Therefore, the difference in the total dephasing rates in the current situation is most likely due to the shorter vibrational lifetime of the $v = 2$ level than that of the $v = 1$ level [31]. The lifetime of the $v = 1$ level measured by a pump–probe experiment is 12.6 ps at 80 K, which yields a pure dephasing rate of $\sim 1/(44 \text{ ps})$ for 0–1 transition. By assuming the same pure dephasing rates for the 0–1 and 1–2 transitions, the lifetime of the $v = 2$ level is estimated to be 6.2 ps. The ratio of the lifetimes of the two vibrational levels, $T_{1, v = 1}/T_{1, v = 2}$, is 2.05, very close to 2.0 predicted for a harmonic oscillator.

Vibrational echoes measure the homogeneous linewidth and, thus, separate the homogeneous and inhomogeneous broadening. The fact that single exponential echo decay is obtained for 0–1 transition suggests that the solvent motion in this system can be well separated into homogeneous broadening and inhomogeneous broadening and that the homogeneous part is in the motional narrowing limit [33]. The echo decay rate of 4.0 ps at 80 K for the 0–1 transition corresponds to a homogeneous linewidth of 0.65 cm^{-1} if the line is substantially inhomogeneously broadened and 1.3 cm^{-1} if the line is homogeneously broadened. Because both of these values are much smaller than the total absorption linewidth (22.8 cm^{-1}), it is clear that the absorption line is massively inhomogeneously broadened. The vibrational dephasing in this system can be modeled as a small amount of homogenous broadening (which is motionally narrowed) imbedded in a inhomogeneously broadened absorption line. This is consistent with what might be expected for a chromophore imbedded in a polymer matrix such as PMMA at low temperatures. For this system at 80 K, the frequency-frequency cor-

relation function of the solvent fluctuations can be written as

$$\langle \delta\omega_{10}(\tau_2)\delta\omega_{10}(0) \rangle = \Delta_h^2 \exp(-t/\tau_h) + \Delta_{\text{in}}^2, \quad (7)$$

where Δ_h and τ_h are the solvent fluctuation magnitude and time scale, respectively, for the homogenous line, and Δ_{in} is the inhomogeneous broadening. The pure dephasing rate is given by the product $\Delta_h^2 \tau_h$. Because the pure dephasing rate and thus the echo decay rate depend only on the product in the motional narrowing limit ($\Delta\tau = 1$), the values of Δ_h and τ_h cannot be obtained independently.

One possible mechanism that could give rise to the data at 80 K is the phonon-induced motion, or the so-called inertial motion. In this mechanism, it is assumed that fast phonon fluctuations are relatively strongly coupled to the vibrational transition and that other motions of the glass, such as the rotational and diffusive motions of the polymer matrix, are frozen out. The time scale of the inertial motion has been found to range from 30 to 200 fs for different solvents [38]. To illustrate the results of assuming this mechanism, we take a typical value, that is, $\tau_h = 100$ fs. Then using $\Delta_h^2 \tau_h = 1/T_2^*$, and the experimentally determined value, $T_2^* \sim 44$ ps, gives $\Delta_h = 0.48$ ps^{-1}. $\Delta_{\text{in}} = 1.8$ ps^{-1} is obtained from the simulation of the linear absorption spectrum. Using these parameters, we can simulate both the 1-D and frequency-selected vibration echo. The main purpose of the calculations is to reproduce the 1-D and frequency-selected vibrational echo decays. It is important to emphasize that a choice of a different physical mechanism for the dephasing could yield different values of τ_h and Δ_h, but the results of the calculations of the wavelength dependence of the vibrational echo decays would be unchanged.

Figure 5 displays the results of the calculations that mimic the data taken in the PMMA solvent at 80 K. For the simplicity, the simulation is carried out in the impulsive limit (infinitely short pulse duration) and only the positive part is considered (only R_1, R_2 and R_3 are included in the simulation of 1-D and frequency-selected echoes). Figure 5a shows the absorption spectrum and the calculation of absorption spectrum through Eq. (2), with additional lifetime broadening also included. The calculations of the echo signals are based on Eq. (5) (1-D) and Eq. (6) (frequency-selected) with the lifetime effect included as discussed in Section 2. The parameters used in all the simulations are identical and were obtained from the experimental results discussed above. The frequency-frequency correlation function is assumed to be $\langle \delta\omega_{10}(\tau_2)\delta\omega_{10}(0) \rangle = \Delta_h^2 \exp(-t/\tau_h) + \Delta_{\text{in}}^2$, with $\Delta_h = 0.48$ ps^{-1}, $\tau_h = 100$ fs and $\Delta_{\text{in}} = 1.8$ ps^{-1}. The lifetimes $T_{1, v = 1} = 12.6$ ps and $T_{1, v = 2} = 6.2$ ps are used in the simulations. The center frequency of 0–1 transition is 1948 cm^{-1}. Figure 5b is a
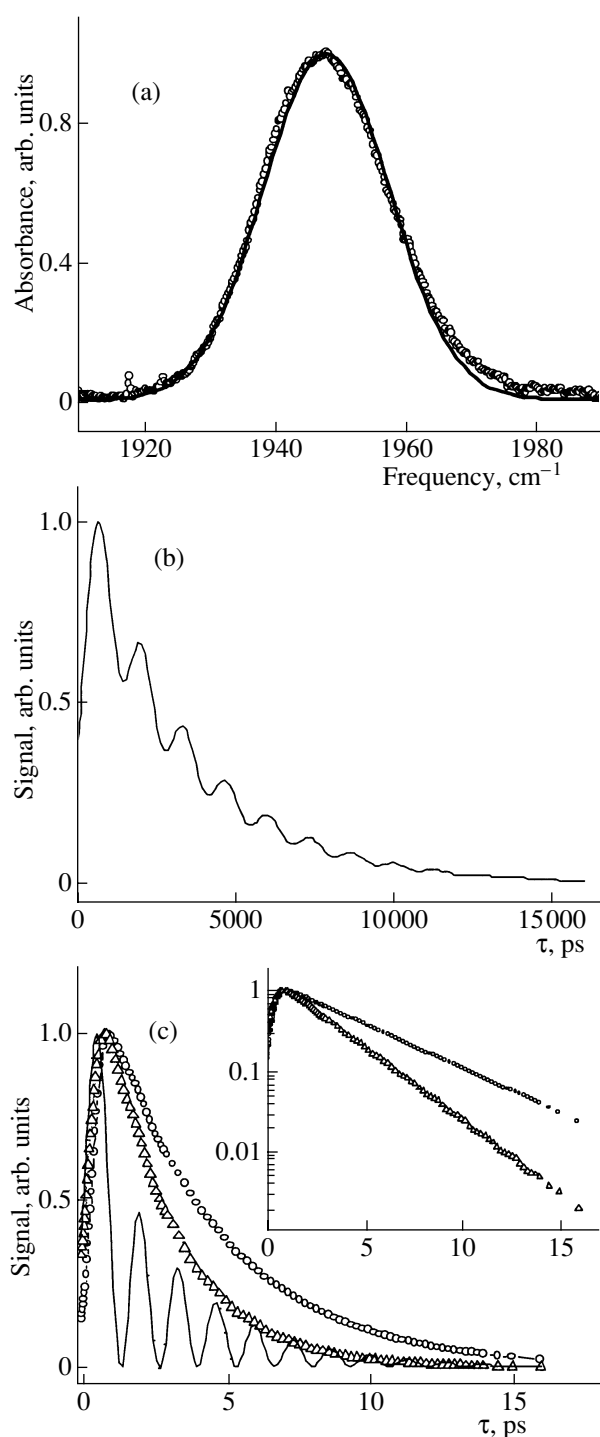
Fig. 5. Simulation of the linear and nonlinear spectra. The frequency-frequency correlation function is taken to be

$$\langle\delta\omega_{10}(\tau_2)\delta\omega_{10}(0)\rangle \;=\; \Delta_h^2 \exp(-t/\tau_h) \;+\; \Delta_{in}^2,$$

with $\Delta_h = 0.48$ ps^{-1}, $\tau_h = 100$ fs and $\Delta_{in} = 1.8$ ps^{-1}. The lifetimes $T_{1,\,v=1} = 12.6$ ps and $T_{1,\,v=2} = 6.2$ ps are used in the simulations. (a) Simulated (solid line) and experimental (symbol) linear absorption spectrum; (b) Simulated 1-D echo signal; (c) Simulated frequency-selected vibrational echo at 1954 cm^{-1} (circles), 1935 cm^{-1} (solid line) and 1918 cm^{-1} (triangles). The inset is the semi-log plot of the simulated 1954 and 1918 cm^{-1} results.

calculation of the 1-D echo decay. Of particular interest is the calculation of frequency-selected vibrational echo data shown in Fig. 5c. The top most curve is calculated for a detection wavelength of 1954 cm^{-1} ($\omega = 6$ cm^{-1}). The decay is a single exponential (top curve in the inset) without beats. The middle curve is calculated for a detection wavelength of 1918 cm^{-1} ($\omega = -30$ cm^{-1}). Again, a single exponential decay (bottom curve in the inset) without beats is obtained. The lowest curve, which is highly modulated, was calculated for a detection wavelength of 1935 cm^{-1} ($\omega = -13$ cm^{-1}). In contrast to the other two curves in Fig. 5c, there are beats with almost 100% depth of modulation. The calculations reproduce the linear spectrum (Fig. 5a), and comparing to Figs. 2 and 4, they also reproduce the 1-D (Fig. 5b) and frequency selected data (Fig. 5c) extremely well, even though the phenomenological parameters obtained from the experiments but based on the two-level model system were used in the simulations. The consistence of the simulation results with data suggests that the frequency selected echo signal of a three-level system, when the proper detection wavelength is selected, can be modeled as a pseudo two-level system.

4.2. FSVE Study of RuTPPCOPy in Liquid 2-MTHF

Figure 6 displays data taken on RuTPPCOPy/2-MTHF. Figure 6a shows the 0–1 absorption spectrum and the 1–2 spectrum modeled as the 0–1 spectrum shifted by the anharmonicity. In contrast to RuTPPCOPy/PMMA, the absorption linewidth is smaller than the anharmonicity; very little spectral overlap exists between the 0–1 and 1–2 transitions. Figure 6b displays 1-D data taken at three temperatures (80, 100, and 280 K, top curve to bottom curve). Because the inhomogeneous broadening is small compared to the anharmonicity, no obvious anharmonic beats are observed in the 1-D data, even when the temperature is below the glass transition temperature (80 K data) [17, 19]. Nonetheless, for positive delay times all of the terms R_1/R_2 and R_3 (Fig. 1a) contribute to the echo signals, and the decays reflect the combined dephasing dynamics of the 0–1 and 1–2 transitions. The lack of beats in the 1-D decays is consistent with the theoretical prediction that the spectral overlap between 0–1 and 1–2 transitions is a prerequisite to see anharmonic beats that arise from interference between the R_1/R_2 and R_3 terms in the 1-D echo signal. (Under the right circumstances, it is possible to see anharmonic beats when there is spectral overlap with another vibrational transition of the molecule or if there is spectral overlap with a vibrational transition of a different molecule [19].) In the frequency selected experiment (Fig. 6c), setting the detection wavelengths to the peaks of the 0–1 and 1–2 transitions, yields the dephasing dynamics solely associated with R_1/R_2 and R_3 terms, respectively. At high temperatures (e.g., 280 K, Fig. 6c), the vibrational echo decay profiles associated

with R_1/R_2 (filled squares) and R_3 (open circles) terms display strongly non-exponential behavior that is virtually identical for positive delays. This supports the conclusion drawn above that the pure dephasing rates associated with 0–1 and 1–2 transitions are very similar, and the difference in the decays for the 0–1 and 1–2 transitions at low temperatures (Fig. 4) arises from difference in the lifetimes. At 280 K in 2-MTHF, the lifetime makes a negligible contribution to the vibrational echo decay (the lifetime of $v = 1$ level is ~16 ps at 280 K).

It is frequently assumed that a vibration in a liquid at or near room temperature is homogeneously broadened, since the solvent motion will be expected to become faster and the absorption line shape becomes more Lorentzian as the temperature increases. When the vibrational line is entirely homogeneously broadened, the solvent motion will cause the vibrational transition to be in the motional narrowing limit, the spread in frequencies is averaged into a Lorentzian line (linear spectrum), and the vibrational echo decay is exponential [39, 40]. The non-exponential decay observed at high temperatures in liquid 2-MTHF demonstrates that the above simple picture does not apply to this system in the liquid at 280 K. The functional form of the decay and the rate of the decay show that CO stretching mode of RuTPPCOPy/2-MTHF is not completely homogeneously broadened at 280 K (or room temperature). Instead, the solvent modulation of the vibrational transition frequency occurs on a variety of time scales. In the PMMA glass, a relatively narrow homogeneous line is imbedded in a large amount of inhomogeneity. The same description also applies in 2-MTHF near the glass transition temperature (86 K) and in the glass. The inset in Fig. 6b shows the 0–1 data taken at 100 K on a semi-log plot; the echo decay is found to be single exponential. As discussed above, one possible source of the motional narrowing in the glass is the phonon (inertial) motions of the medium that have a very short correlation time, τ_h. When the temperature is raised above the glass transition temperature in 2-MTHF, motions of the small solvent molecules will no longer be frozen out, and the diffusive motions of the solvent (both translations and rotations) will contribute to the vibrational echo signal decay. These diffusive motions will become faster as the temperature increases. Even though the absorption line width at 280 K in 2-MTHF is narrower than that in PMMA (thus, a slower echo decay might be expected in 2-MTHF), comparing the 1-D data at 280 K in PMMA and 2-MTHF (Figs. 2 and 6b) shows that the 1-D echo decay in 2-MTHF is significantly faster than in PMMA. The similar faster decay in 2-MTHF than in PMMA at same temperature is also observed in the frequency-selected vibrational echo (Fig. 7). These observations add to the evidence that in 2-MTHF, additional dephasing due to diffusive motions, which are potentially frozen in PMMA, also contributes to the echo decay. At high temperatures, the solvent modulation of the vibrational transition frequency occurs on at least two time scales. Besides the
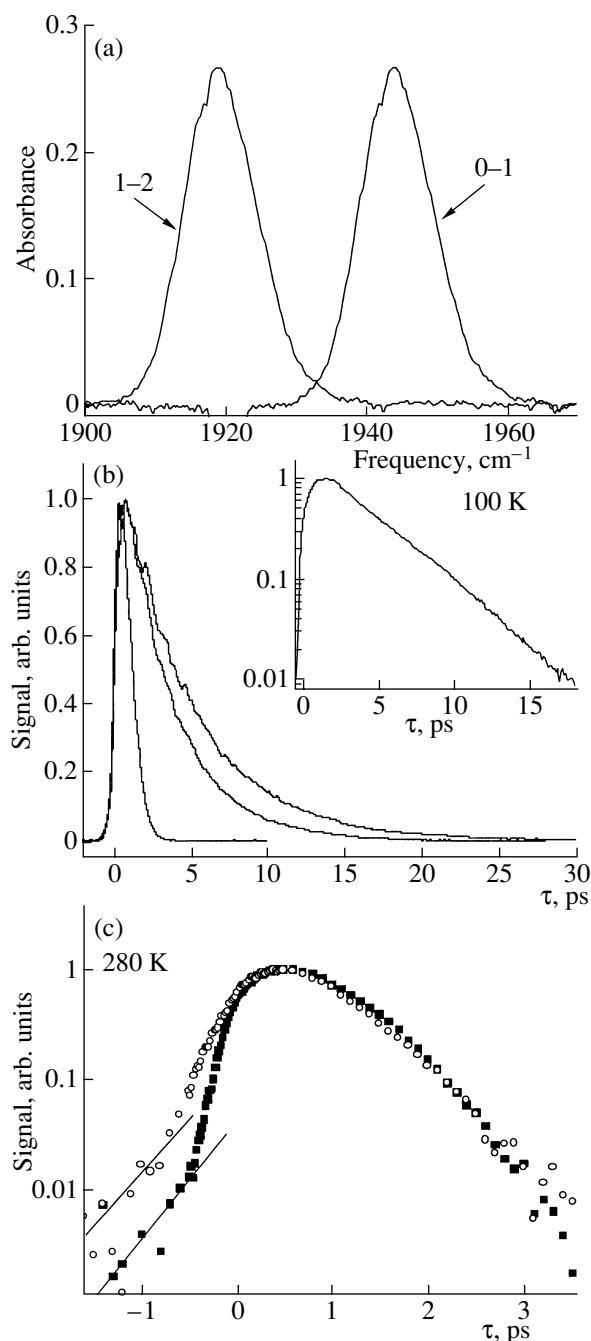
Fig. 6. Data for RuTPPCOPy in 2-MTHF. (a) The absorption spectrum at 100 K labeled 0–1. The curve labeled 1–2 is a model of the 1–2 absorption spectrum obtained by shifting the 0–1 transition by the anharmonic shift (23 cm^{-1}). (b) 1-D vibrational echo decays at (from top to bottom) 80, 100, and 280 K. There are no anharmonic beats because of the very small spectral overlap of the 0–1 and 1–2 lines. The inset shows that the low temperature (100 K) 0–1 data decay is an exponential. (c) Frequency selected vibrational echo decays (slices through the 2-D spectrum) at 280 K detected at the peaks of the 0–1 (squares) and 1–2 (circles) transitions. The decays at positive delays are virtually identical and non-exponential. At negative delays, the relative amplitude of the 1–2 signal is larger than the 0–1 signal when the signals are matched at their maxima. The two lines at negative delay times are an aid to the eye to indicate that the negative time signals are very similar in functional form.

Signal, arb. units
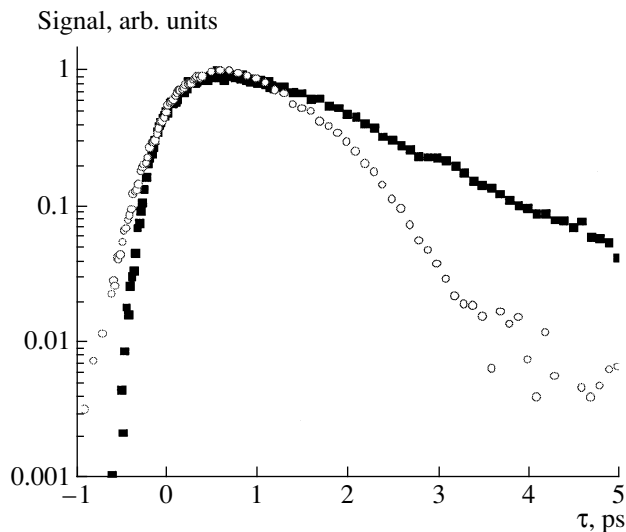
Fig. 7. The demonstration of the effect of the inhomogeneity on the negative time delay signals: RuTPPCOPy in 2-MTHF (open circles) and PMMA (solid squares) at 200 K. The wavelength was chosen to correspond to the 1–2 transition. It can be seen at negative times, larger signals is observed in 2-MTHF than in PMMA. However, at positive times, the echo decay in 2-MTHF is found to be faster than that in PMMA.

fast phonon-induced (inertial) motion, the diffusive solvent motion will also modulate the vibrational transition frequency. The fast phonon-induced motion is usually in the motional narrowing limit, while the diffusive motion could be on the time scale of subpicoseconds to hundreds of picoseconds depending on the solvent property and temperature [41], and is usually not in the motional narrowing limit. Having multiple time scales will result in a non-exponential decay. As mentioned earlier, sorting out the dynamics from such non-exponential decays would be virtually impossible to do in a conventional 1-D experiment. The details of the effect of the temperature dependence of the inertial motion and diffusive motion on echo signal will be presented elsewhere [42].

Another unusual feature of the vibrational echo decay data taken in 2-MTHF is that significant signals were observed in the negative time region (Fig. 6c). The signals at negative times are significantly larger than those observed in the PMMA solvent (see Fig. 7). Such signals are due to the contributions from the R_7 and R_8 terms in Fig. 1. Since R_7 and R_8 are non-rephasing terms, their contributions will be minimized when a large amount of inhomogeneity exists. The negative time signal in 2-MTHF is significantly larger than that in PMMA because the inhomogeneity in the PMMA polymer matrix large compared to that in 2-MTHF. Observation of a large negative time signal is usually an indication that the system has only a small degree of inhomogeneous broadening. Inspection of the vibrational echo signals at the two wavelengths (Fig. 6c) cor-

responding to the 0–1 (squares) and 1–2 (circles) transitions, shows that the signal at the 1–2 detection wavelength is larger in the negative time delay region than the 0–1 signal when the signals are matched at their peaks. This difference in amplitude is observed at a variety of temperatures. When the detection wavelength is close to the peak of the 0–1 transition, R_1, R_2, R_4, R_5, R_7 contribute to the total signal, and R_7 and the rising edges of the other four terms will contribute to the signal at negative time delay. When the detection wavelength is located at the peak of 1–2 transition, R_3, R_6 and R_8 contribute to the total signal, and R_8 and the rising edges of other two terms contribute to the signal at negative delays. At significant negative delay, the signal arises only from R_7 for the 0–1 detection wavelength and only from R_8 for the 1–2 detection wavelength. The mechanism responsible for the different signal amplitudes at negative delay times is unknown. Both the R_7 and R_8 terms involve 0–1 and 1–2 transitions to the same extent and should give equal contributions to the negative delay signals. In the harmonic approximation, the transition dipole matrix element for the 2–1 transition is $\sqrt{2}$ bigger than that for the 1–0 transition. At the signal level, (matrix element squared), the sum of R_1 and R_2 (or R_4 and R_5) will give the same amount of the signal as that of R_3 (or R_6). After normalization at the peak of the signal, the same amount of signal would be expected at both detection wavelengths at negative delay times. It is also worth noting that the negative time delay signals involve a 2–0 coherence. In principle, information on the decay of the 2–0 coherence can be obtained from analysis of the negative time delay signals.

5. CONCLUDING REMARKS

Ultrafast infrared vibrational echo experiments inherently involve pulses with bandwidths that can exceed the vibrational anharmonicity and other vibrational splittings. Frequently, the information that is desired from a vibrational echo experiment is the dynamics of a particular transition. Comparison of the vibrational echo decays in Figs. 2 and 4 demonstrates that spectrally resolving the vibrational echo and detecting the signal at particular wavelengths (frequency-selected vibrational echo) can simplify the nature of the decays and provide the desired information directly.

Frequency-selected vibrational echo studies of the CO stretching mode of RuTPPCOPy permitted comparison of the vibrational echo decays of the 0–1 (fundamental) and the 1–2 transitions. The FSVE decay signal of the 0–1 transition of RuTPPCOPy in PMMA polymer matrix is single exponential, suggesting that a motionally narrowed homogeneous dephasing process is imbedded in vibrational absorption line with a substantial degree of inhomogeneity. The dephasing of the

1–2 transition is faster than that of 0–1 transition at low temperature due to significant contributions from vibrational population relaxation and the shorter lifetime of $v = 2$ compared to $v = 1$ states. A simulation based on the phenomenological parameters obtained above was performed (Fig. 5) that reproduced the data for the linear spectrum and the nonlinear 1-D and frequency-selected vibrational echo decays.

In contrast, in 2-MTHF liquid, the decays associated with 0–1 transition is exponential at low temperatures but non-exponential at high temperatures (Fig. 6c). The dephasing dynamics for 0–1 and 1–2 transitions at high temperatures are dominated by pure dephasing and are virtually identical. The non-exponential decays show that, even in a high temperature liquid, the vibrational absorption lines are not motionally narrowed, homogeneously broadened transitions. Instead, the data suggest that a multitude of the time scales of solvent modulation contribute to the linear spectrum and nonlinear vibrational echo signals. The temperature dependence of the vibrational dephasing of RuTPPCOPy in PMMA and 2-MTHF and the underlying dephasing mechanisms will be discussed in detail subsequently [42].

REFERENCES

1. Hahn, E.L., 1950, *Phys. Rev.*, **80**, 580.
2. Kurnit, N.A., Abella, I.D., and Hartmann, S.R., 1964, *Phys. Rev. Lett.*, **13**, 567.
3. Abella, I.D., Kurnit, N.A., and Hartmann, S.R., 1966, *Phys. Rev.*, **14**, 391.
4. Lvovsky, A.I. and Hartmann, S.R., 1996, *Laser Phys.*, **6**, 535.
5. Zimdars, D., Tokmakoff, A., Chen, S., Greenfield, S.R., Fayer, M.D., Smith, T.I., and Schwettman, H.A., 1993, *Phys. Rev. Lett.*, **70**, 2718.
6. Horng, M.L., Gardecki, J.A., Papazyan, A., and Maroncelli, M., 1995, *J. Phys. Chem.*, **99**, 17311.
7. Rullière, C., 1998, *Femtosecond Laser Pulses: Principles and Experiments* (Berlin: Springer).
8. Larsen, D.S., Ohta, K., Xu, Q.H., Cyrier, M., and Fleming, G.R., 2001, *J. Chem. Phys.*, **114**, 8008.
9. Book, L.D. and Scherer, N.F., 1999, *J. Chem. Phys.*, **111**, 792.
10. Ohta, K., Larsen, D.S., Yang, M., and Fleming, G.R., 2001, *J. Chem. Phys.*, **114**, 8020.
11. Zimdars, D., Tokmakoff, A., Chen, S., Greenfield, S.R., Fayer, M.D., Smith, T.I., and Schwettman, H.A., 1993, *Phys. Rev. Lett.*, **70**, 2718.
12. Tokmakoff, A. and Fayer, M.D., 1995, *Acc. Chem. Res.*, **28**, 437.
13. Rector, K.D. and Fayer, M.D., 1998, *Int. Rev. Phys. Chem.*, **17**, 261.
14. Rector, K.D. and Fayer, M.D., 1998, *J. Chem. Phys.*, **108**, 1794.
15. Asplund, M.C., Lim, M., and Hochstrasser, R.M., 2000, *Chem. Phys. Lett.*, **323**, 269.
16. Zanni, M.T., Asplund, M.C., and Hochstrasser, R.M., 2001, *J. Chem. Phys.*, **114**, 4579.
17. Thompson, D.E., Merchant, K.A., and Fayer, M.D., 2001, *J. Chem. Phys.*, **115**, 317.
18. Merchant, K.A., Thompson, D.E., and Fayer, M.D., 2001, *Phys. Rev. Lett.*, **86**, 3899.
19. Merchant, K.A., Thompson, D.E., and Fayer, M.D., 2002, *Phys. Rev. A*, **65**, 023817.
20. Golonzka, O., Khalil, M., Demirdoven, N., and Tokmakoff, A., 2001, *Phys. Rev. Lett.*, **86**, 2154.
21. Demirdoven, N., Khalil, M., Golonzka, O., and Tokmakoff, A., 2001, *J. Phys. Chem. A*, **105**, 8030.
22. Khalil, M. and Tokmakoff, A., 2001, *Chem. Phys.*, **266**, 213.
23. Rella, C.W., Rector, K.D., Kwok, A.S., Hill, J.R., Schwettman, H.A., Dlott, D.D., and Fayer, M.D., 1996, *J. Phys. Chem.*, **100**, 15620.
24. Rector, K.D., Engholm, J.R., Rella, C.W., Hill, J.R., Dlott, D.D., and Fayer, M.D., 1999, *J. Phys. Chem. A*, **103**, 2381.
25. Rector, K.D., Jiang, J., Berg, M., and Fayer, M.D., 2001, *J. Phys. Chem. B*, **105**, 1081.
26. Rector, K.D., Rella, C.W., Kwok, A.S., Hill, J.R., Sligar, S.G., Chien, E.Y.P., Dlott, D.D., and Fayer, M.D., 1997, *J. Phys. Chem. B*, **101**, 1468.
27. Asplund, M.C., Zanni, M.T., and Hochstrasser, R.M., 2000, *Proc. Natl. Acad. Sci. USA*, **97**, 8219.
28. Fayer, M.D., 2001, *Annu. Rev. Phys. Chem.*, **52**, 315.
29. Tokmakoff, A. and Fayer, M.D., 1995, *J. Chem. Phys.*, **103**, 2810.
30. Tokmakoff, A., Kwok, A.S., Urdahl, R.S., Francis, R.S., and Fayer, M.D., 1995, *Chem. Phys, Lett.*, **234**, 289.
31. Rector, K.D., Kwok, A.S., Ferrante, C., Tokmakoff, A., Rella, C.W., and Fayer, M.D., 1997, *J. Chem. Phys.*, **106**, 10027.
32. Merchant, K.A., Thompson, D.E., Xu, Q.-H., Loring, R.F., and Fayer, M.D., 2002, *Biophys. J.*, **86**, 3277.
33. Mukamel, S., 1995, *Principles of Nonlinear Optical Spectroscopy* (New York: Oxford Univ. Press).
34. Hamm, P., Lim, M., and Hochstrasser, R.M., 1998, *Phys. Rev. Lett.*, **81**, 5326.
35. Arrivo, S.M., Dougherty, T.P., Grubbs, W.T., and Heilweil, E.J., 1995, *Chem. Phys. Lett.*, **235**, 247.
36. Fourkas, J.T., Kawashima, H., and Nelson, K.A., 1995, *J. Chem. Phys.*, **103**, 4393.
37. Hill, J.R., Rosenblatt, M.M., Ziegler, C.J., Suslick, K.S., Dlott, D.D., Rella, C.W., and Fayer, M.D., 1996, *J. Phys. Chem.*, **100**, 18023.
38. Passino, S.A., Nagasawa, Y., Joo, T., and Fleming, G.R., 1997, *J. Phys. Chem. A*, **101**, 725.
39. Farrar, T.C. and Becker, D.E., 1971, *Pulse and Fourier Transform NMR* (New York: Academic).
40. Berg, M.A., Rector, K.D., and Fayer, M.D., 2000, *J. Chem. Phys.*, **113**, 3233.
41. Berg, M.A. and Hubble, H.W., 1998, *Chem. Phys.*, **233**, 257.
42. Xu, Q.-H. and Fayer, M.D., 2002, *J. Chem. Phys*. (in press).